Received: 18 January 2022 | Accepted: 15 February 2022

DOI: 10.1002/rmb2.12452

Reproductive Medicine and Biology

WILEY

ORIGINAL ARTICLE

Loss of *Axdnd1* causes sterility due to impaired spermatid differentiation in mice

Yuki Hiradate[1] | Ryua Harima[1] | Rin Yanai[1] | Kenshiro Hara[1] | Kazue Nagasawa[2] | Makoto Osada[2] | Tomoe Kobayashi[3] | Makoto Matsuyama[3] | Shin-ichiro Kanno[4] | Akira Yasui[4] | Kentaro Tanemura[1]

[1]Laboratory of Animal Reproduction and Development, Graduate School of Agricultural Science, Tohoku University, Sendai, Japan

[2]Laboratory of Aquacultural Biology, Graduate School of Agricultural Science, Tohoku University, Sendai, Japan

[3]Division of Molecular Genetics, Shigei Medical Research Institute, Okayama, Japan

[4]Division of Dynamic Proteome and IDAC Fellow Research Group for DNA Repair and Dynamic Proteome Institute of Development, Aging and Cancer (IDAC), Tohoku University, Sendai, Japan

Correspondence
Kentaro Tanemura, Laboratory of Animal Reproduction and Development, Graduate school of Agricultural Science, Tohoku University, Aramaki 468-1, Sendai 980-8572, Japan.
Email: kentaro.tanemura.e4@tohoku.ac.jp

Present address
Yuki Hiradate, Department of Experimental Genome Research, Research Institute for Microbial Diseases, Osaka University, Osaka, Japan

Funding information
This study is supported by Japan Society for the Promotion of Science (JSPS) Grants, 20K06442 to YH., 21H02341 to KH., 19H01142 to KT., and by Support Program for Interdisciplinary Research by Frontier Research Institute for Interdisciplinary sciences, Tohoku University to KT

Abstract

Purpose: Spermiogenesis, the process of deformation of sperm head morphology and flagella formation, is a phenomenon unique to sperm. Axonemal dynein light chain proteins are localized to sperm flagella and are known to be involved in sperm motility. Here, we focused on the gene axonemal dynein light chain domain containing 1 (*Axdnd1*) with the aim to determine the function of its protein product AXDND1.

Methods: To elucidate the role of AXDND1 in spermatogenesis, we generated *Axdnd1* knockout (KO) mice using the CRISPR/Cas9 system. The generated mice were subjected to fertility tests and analyzed by immunohistochemistry.

Result: The *Axdnd1* KO mouse exhibited sterility caused by impaired spermiogenesis during the elongation step as well as abnormal nuclear shaping and manchette, which are essential for spermiogenesis. Moreover, AXDND1 showed enriched testicular expression and was localized from the mid-pachytene spermatocytes to the early spermatids.

Conclusion: *Axdnd1* is essential for spermatogenesis in the mouse testes. These findings improve our understanding of spermiogenesis and related defects. According to a recent report, deleterious heterozygous mutations in AXDND1 were found in non-obstructive azoospermia (NOA) patients. Therefore, *Axdnd1* KO mice could be used as a model system for NOA, which will greatly contribute to future NOA treatment studies.

KEYWORDS
AXDND1, manchette, nuclear shaping, spermiogenesis, sterility

Yuki Hiradate and Ryua Harima are co-first authors and also equally contributed to this study.

1 | INTRODUCTION

Spermatogenesis is a complex and dynamic process. Differentiated spermatocytes must undergo meiosis, during which the nuclear phase of the cells shifts from diploid (2C) to haploid (1C) via 4C. Spermiogenesis, which involves sperm head shaping and flagella formation, is a phenomenon characterized by unique and drastic changes in cell morphology,[1] such as chromatin compaction by replacing histones with protamine[2] and acrosome formation.[3] In this process, the components of proteins necessary to build the flagella are transported on railed microtubules associated with intraflagellar transporter proteins (IFT)[4–6] and motor proteins[7,8] to elongate flagella[9,10] with the removal of the cytoplasm.[11] This same microtubule-based skirt-like transient structure called the manchette is supposed to play an important role in protein delivery and sperm head shaping.[1,12]

Mammalian testes express specific genes required to regulate complex sperm differentiation processes. However, the functions of proteins encoded by these genes are unknown.[13–15] Therefore, elucidation of individual gene functions and accumulation of knowledge is required for an integrated understanding of spermatogenesis. Indeed, DNA analysis of patients with infertility has elucidated the associated genetic factors.[16] Furthermore, the use of a knockout (KO) mouse model by the development of a simplified method using the CRISPR/Cas9 system allows for determination of required gene products.[17,18]

Here, we focused on mouse *Axdnd1* (axonemal dynein light chain domain containing 1), which is an orthologous gene of human *AXDND1*(*C1orf125*). However, despite its expression in the testes, its function is yet to be characterized. To uncover the requirement of the protein product AXDND1 in spermatogenesis, we generated gene KO mice. It has recently been shown that *Axdnd1*-deficient male mice display infertility.[19] However, AXDND1 had not been analyzed using antibodies against this protein, so we aim to reveal the localization pattern of AXDND1 in spermatogenesis via immunostaining using a home-grown antibody and to deepen our understanding of the function of AXDND1.

2 | MATERIALS AND METHODS

2.1 | Animals

C57BL/6N mice were purchased from SLC and maintained under a 12-h light/dark cycle.

2.2 | Chemicals

All reagents were purchased from Nacalai Tesque unless otherwise stated.

2.3 | Preparation of antibodies against AXDND1

An antibody against AXDND1 was prepared using a recombinant protein as outlined previously.[20] The partial cDNA sequence of AXDND1(CCDS83611.1) corresponding to 958–1111 aa was amplified by PCR, inserted into the His-tagged pCold-pros2 vector (Takara Bio), and transformed into DH5a competent *E. coli* (Takara Bio). The selected clone was further transformed into the BL21 (DE3) *E. coli* strain (Takara Bio), and protein expression was induced with IPTG. After the tagged protein was eluted with imidazole and enzymatically digested by HRV3C protease, the pros2 tag was removed, and the purified protein was immunized into rabbits to produce polyclonal antibodies. The resulting IgG-purified antiserum was used in this study.

2.4 | mRNA and protein expression patterns in tissues

cDNA libraries were obtained from several tissues, and mRNA expression was analyzed. Tissues collected and stored for RNA extraction were homogenized in Sepazol. Total RNA was isolated according to the manufacturer's instructions. A total of 500 ng of total RNA were reverse-transcribed (Revertra ace; Toyobo) and used for PCR along with the appropriate paired primers for *Axdnd1* (F: 5′- AAAGACCTGGTGACTCAGCG-3′ and R: 5′-GTCATTAAGGGCTACGGCGA-3′ [generated 636 bp]) and β-actin (F: 5′-AAGAGCTATGAGCTGCCTGA-3′ and R: 5′-CAGGAGGAGCA ATGATCTTG-3′ [generated 270 bp]). The designed primer pair spanned different exons. The cycling program was as follows: 94°C for 3 min, denaturation at 94°C for 10 s, 35 cycles of annealing at 55°C for 15 s, extension at 68°C for 20 s, and further extension at 68°C for 5 min.

From tissues (8–12 weeks old mice), proteins were extracted using RIPA buffer containing 1% protease inhibitor (Nacalai Tesque, #25955) and the concentration was measured using the BCA method. A total of 10 μg proteins were separated by SDS-PAGE, transferred to a PVDF membrane, and treated with a commercial blocking buffer (Blocking One Nacalai Tesque) for 1 h at room temperature (RT). The membranes were subsequently washed with TBS containing 0.1% Tween 20 (TBS-T) and incubated with anti-AXDND1 antiserum (1:2000) or anti-β-actin (1:5000; Santa Cruz Biotechnology, #SC-47778) overnight at 4°C. After washing twice with TBS-T for 5 min each, they were further incubated with anti-rabbit HRP-conjugated antibody (1:2000; Promega #W4011) for 2 h at RT, followed by the addition of HRP substrate. Images were captured using the LAS 3000 imaging system (Fujifilm).

2.5 | Generation of *Axdnd1* KO mice

Axdnd1 KO mice of the C57BL/6N strain were generated by iGONAD as previously reported.[21] Briefly, crRNA was designed with the following sequence: TGTCCATCACGTTGCTCAACTGG (underlined PAM sequence) to target exon 7 of the *Axdnd1* allele

because the InterPro database predicted the presence of axonemal dynein light chain domain at position 209–367 that appeared to be important for protein function (Figure 1B). In addition, crRNA and tracrRNA (Integrated DNA Technologies) were annealed at 94°C for 2 min, mixed with Cas9, and injected into the oviduct at E0.7 of plug confirmed mice. DNA genotyping was performed using DNA extracted from the clipped toes. Primer sequences used were F: 5′-ACACTCTCCTTACCCACGGA-3′ and R: 5′-ACCAGTCTGTCCCTTTGATCTT-3′. The PCR product from the mutant gDNA was Sanger sequenced to determine successful deletion. In order to fix the mutation in the strain, the F0 founder was mated with wild type mice (WT), and the resulting F1 heterozygous male and female mice were crossed to obtain an F2 generation containing homozygous mutants. The established strain was maintained by sibling breeding and used in the current study.

2.6 | Fertility test

A single 8-week-old male mouse (WT, *Axdnd1*$^{+/-}$, or *Axdnd1*$^{-/-}$) was caged with two 8-week-old female WT mice for 4 weeks. Mating was verified by confirming the presence of vaginal plugs. The plugged females were then replaced with new mice. Five male mice of each genotype were used in the experiment. Litter size was scored for the females who had plugs.

2.7 | Histological analysis

After measuring the body weights of both WT and *Axdnd1*$^{-/-}$ mice (8–12 weeks old), they were euthanized by cervical dislocation. Testes were then removed and weighed. The testes and epididymis were fixed in Bouin's solution (Sigma-Aldrich) overnight, gradually dehydrated by stepwise substitution with ethanol and xylene at different concentrations, and finally embedded in paraffin. Sections (4-μm-thick) were rehydrated, stained with periodic acid–Schiff (PAS), and examined under a microscope (Olympus BX50).

2.8 | TUNEL assay

Apoptotic cells were counted using a TUNEL assay. The sections were TUNEL-stained using an in situ apoptosis detection kit (Takara Bio #MK500) following the manufacturer's instructions. Briefly, rehydrated sections were treated with proteinase K for 15 min at RT, labeled with FITC-dUTP by TdT enzyme for 1 h at RT, and covered with a glass coverslip. The samples were examined under a fluorescence microscope (Keyence BZ-X710) using 25 randomly chosen seminiferous tubules sections. Merged signals from the counterstained nuclei were counted. Testes samples were collected from three WT and KO mice.

2.9 | Immunohisto- and immunocytochemistry

The collected testes were fixed overnight in 4% PFA-PBS and embedded in paraffin after dehydration. Sections (4-μm-thick) were rehydrated, treated with antigen-retrieval buffer (pH 9.0; Histo VT One; Nacalai Tesque) for 20 min at 90°C, and washed with tap water for 10 min. The sections were then treated with a commercial blocking buffer (Blocking One; Nacalai Tesque) for 1 h at RT and incubated with the AXDND1 antibody (1:200) overnight at 4°C. The samples were washed three times with PBS containing 0.1% Tween 20 (PBS-T) for 5 min and incubated with Alexa Fluor 488 (Thermo Fisher Scientific #A21206) for 1 h at RT. The coverslips were then observed under a fluorescence microscope, as previously described in the TUNEL assay.

For staining of individual cells, samples were prepared as follows: Testes were minced in 1 ml of DMEM using scissors to release cells from seminiferous tubules and were incubated for 30 min at 37°C. The cell suspension was washed by centrifugation and fixed with 4% PFA-PBS for 10 min at RT. After washing three times with PBS, the

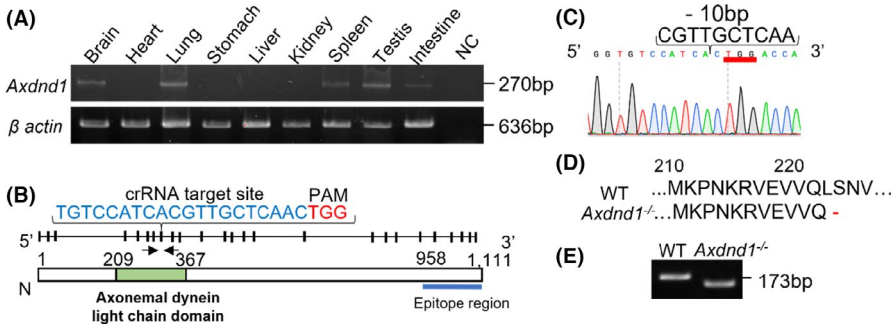

FIGURE 1 mRNA expression profiling and knockout (KO) strategy. (A) *Axdnd1* mRNA expression in mouse tissues as determined by RT-PCR. Total RNA (500 ng) was reverse-transcribed, and cDNA was used for RT-PCR. Deionized water was used as a negative control. (B) Diagram of *Axdnd1* allele and amino acid sequence. Arrows indicate the primer loci designed for genotyping. InterPro database predicted axonemal dynein light chain domain in 209–367 aa. The C-terminal region of 958–1111 aa was referenced for the recombinant protein for antigen. (C) DNA sequence of *Axdnd1*$^{-/-}$ mice. A 10 bp deletion was induced via cocktail injection of crRNA, tracrRNA, and Cas9 protein. Note that mRNA translation occurred in the reverse strand. (D) Disruption of the subsequent in-frame translation 10 bp deletion in the mutated mouse DNA. (E) Patterning of each PCR genotype

suspension was mounted on a glass slide and air-dried. Slides were permeabilized with 0.1% Triton X-100/PBS for 5 min at 37°C, washed again three times with PBS, and treated with blocking solution for 1 h at RT. Afterward, the slides were incubated with primary antibodies overnight at 4°C at the following dilution: α-tubulin (Santa Cruz Biotechnology, #sc-32293: 1:100). The slides were washed three times with PBS and incubated for 1 h at RT. Alexa fluor 568 conjugated lectin PNA (Thermo Fisher Scientific, #L32458:1:200) was used to specify the differentiation stage, and Hoechst 33342 was used for DNA counterstaining.

2.10 | Statistical analysis

The unpaired Student's *t*-test (GraphPad Prism 9; GraphPad Software) was performed for comparison with the WT group. Values are represented as the mean ± SD. Differences were considered significant at $p < 0.05$, indicated as $p < 0.05$ (*) or $p < 0.01$ (**).

TABLE 1 Fertility test of WT, *Axdnd1*$^{+/-}$, and *Axdnd1*$^{-/-}$ male mice

Genotype	*n*	Plugs	Litters	Pups	Pups/Litters
WT	5	47	33	287	8.7 ± 1.3
Axdnd1 $^{+/-}$	5	33	25	208	8.3 ± 1.3
Axdnd1 $^{-/-}$	5	36	0	0	0**

Note: Axdnd1$^{-/-}$ males showed infertility. Each male genotype was mated with two WT females, Plugs: Number of females with plugs in the mating period. Litters: Number of pregnancies. Pups: Total number of each litter. Statistically analyzed pups/litters are shown as mean ± SD. Different letters represent significant differences compared to WT. **; $p < 0.01$.

3 | RESULTS

3.1 | mRNA expression patterns of *Axdnd1*

Axdnd1 mRNA expression patterns in several tissues were compared (Figure 1A). mRNA expression was detected in the brain, lungs, spleen, testes, and intestine.

3.2 | Generation of the mutant mice strain

To understand the contribution of *Axdnd1* to fertility, we generated a KO mouse strain. Specific crRNA targeting the PAM sequence in exon 7 was co-injected with Cas9 protein, and the subsequent 10 bp deletion was confirmed by sequencing (Figure 1C,E). With this deletion, the stop codon (TGA) appeared in frame at the position coding Leu221 (Figure 1D), resulting in termination of translation.

3.3 | *Axdnd1*$^{-/-}$ mouse model showed sterility due to impaired spermatid elongation

The mutant mice were viable and showed no abnormalities. However, fertility tests demonstrated that *Axdnd1*$^{-/-}$ males were

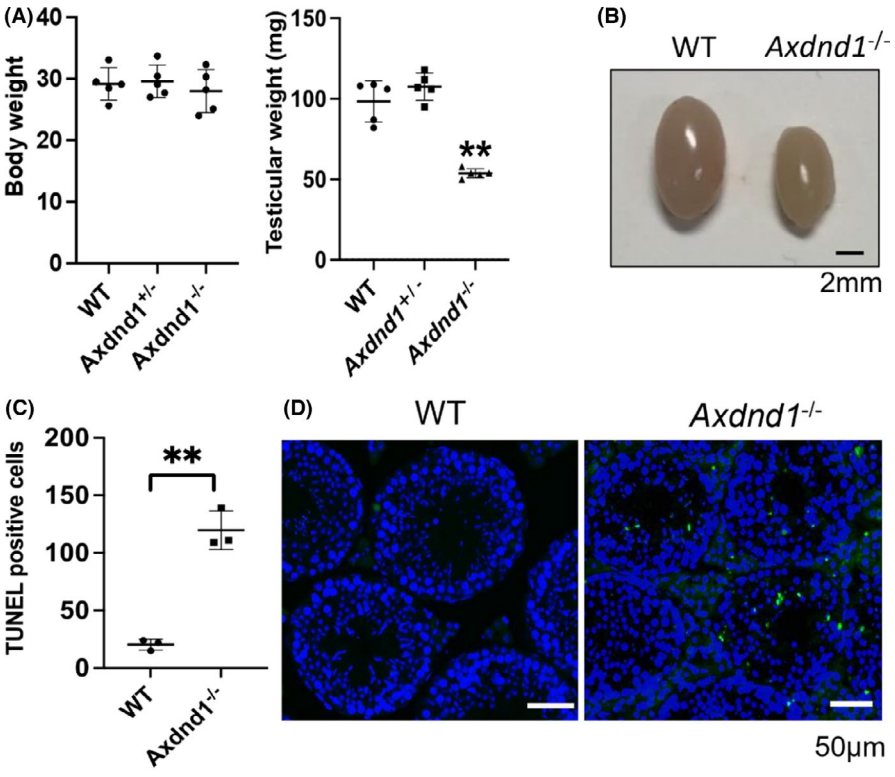

FIGURE 2 *Axdnd1*$^{-/-}$ male testes have smaller size and increased TUNEL-positive cells. (A) Comparison of total body and testes weight for each mouse genotype ($n = 5$). (B) Smaller testes size in *Axdnd1*$^{-/-}$ mice. Representative morphology of WT and *Axdnd1*$^{-/-}$ testes at 8 weeks. Bar = 2 mm. (C) Average number of TUNEL-positive cells in 25 seminiferous tubules of WT and *Axdnd1*$^{-/-}$ testes ($n = 3$). Error bars represent SD. **; $p < 0.01$, ns; no significance. (D) Images showing that frequent TUNEL-positive cells (green) were observed in *Axdnd1*$^{-/-}$ testes counterstained by Hoechst 33342 (blue). Bars =50 μm

sterile, as shown in Table 1. The average number of pups from each genotype was WT: 8.7 ± 1.3, *Axdnd1*$^{+/-}$: 8.3 ± 1.3, and *Axdnd1*$^{-/-}$: 0. Further analysis revealed that the size of the testes of *Axdnd1*$^{-/-}$ mice (53 ± 3 mg) was significantly smaller than that of *Axdnd1*$^{+/-}$ (107 ± 8 mg) and WT (106 ± 11 mg) mice (Figure 2A,B). As the significant decrease in testes weight suggested cell loss,

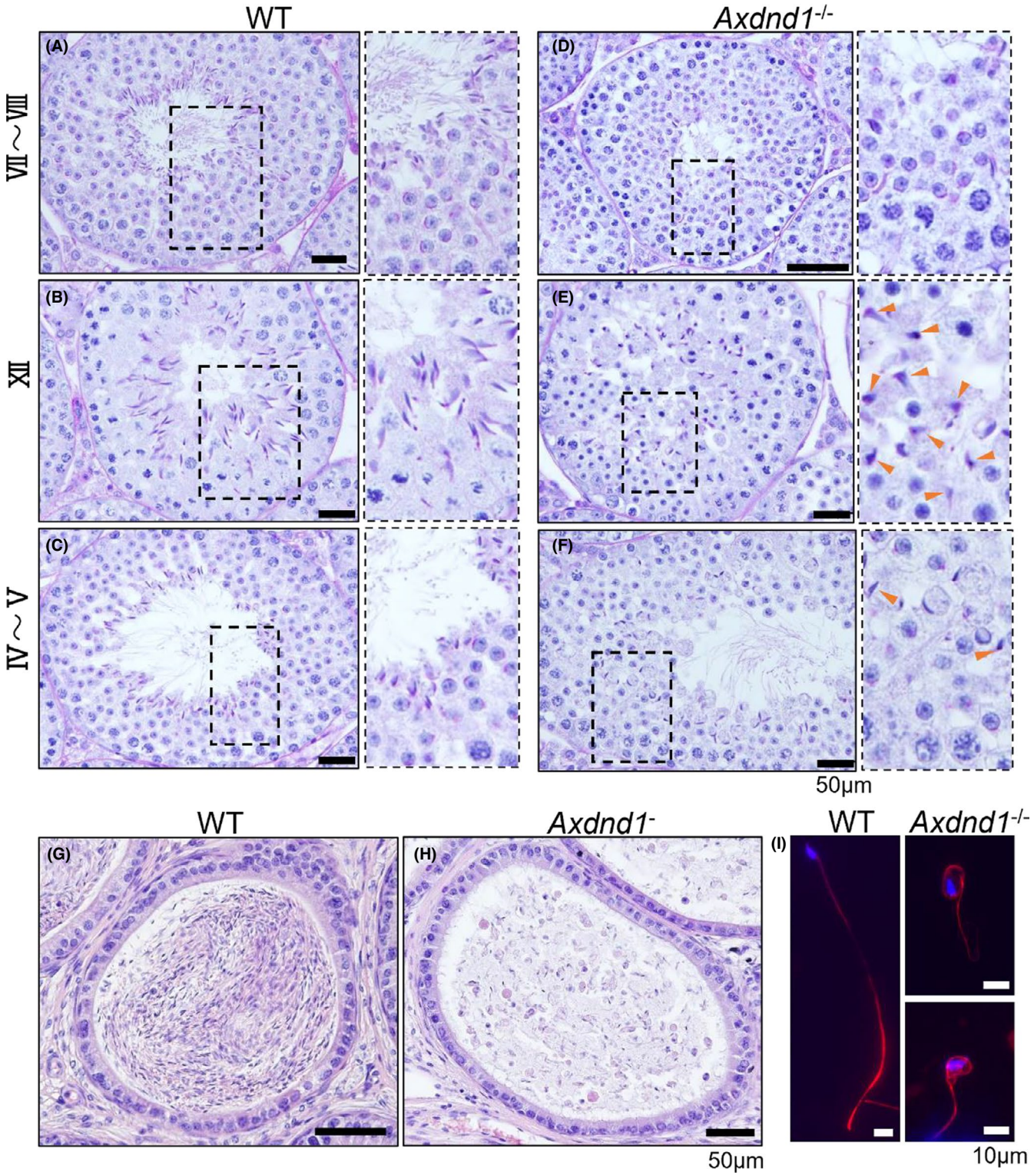

FIGURE 3 *Axdnd1*$^{-/-}$ mice exhibit abnormal spermatogenesis. PAS-stained images of WT vs. *Axdnd1*$^{-/-}$ seminiferous tubules at stage VII ~ VIII (A and D), XII (B and E), and IV ~ V (C and F). Abnormally head-shaped spermatozoa, corresponding to step 12 of spermatids in the XII panel (E; arrows), gradually disappeared in step 15, as shown in stage IV and V panels (F; arrows). WT and *Axdnd1*$^{-/-}$ cauda-epididymis sections (G and H). Few spermatozoa stored in the cauda epididymis (H). Bars = 50 μm. (I) Representative morphology of sperm from the cauda epididymis in WT and *Axdnd1*$^{-/-}$ mice. Nuclei and flagella stained with acetylated α-tubulin (red) or DNA (blue). Bars = 10 μm

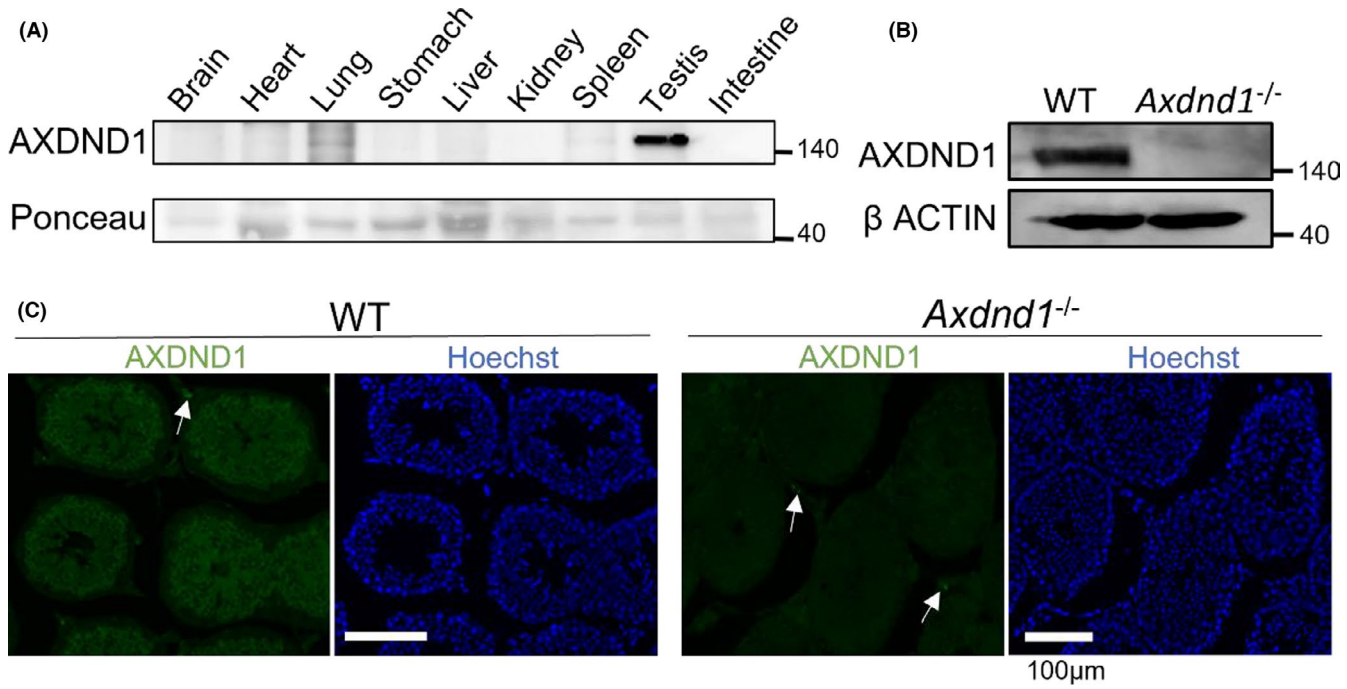

FIGURE 4 Validation of the specificity of the AXDND1 antibody. (A) Analysis of AXDND1 expression in whole tissues. From each tissue, 10 μg of protein was used for SDS-PAGE. Ponceau staining to validate the sample loading. (B) Confirming protein loss of AXDND1 in the mutant testes. (C) Validation of anti-AXDND1 antibody for specific immunostaining. KO section testes-stained same condition is shown as negative control. Arrows indicate the non-specific signals. AXDND1 (Green), DNA (Blue). Bars = 100 μm

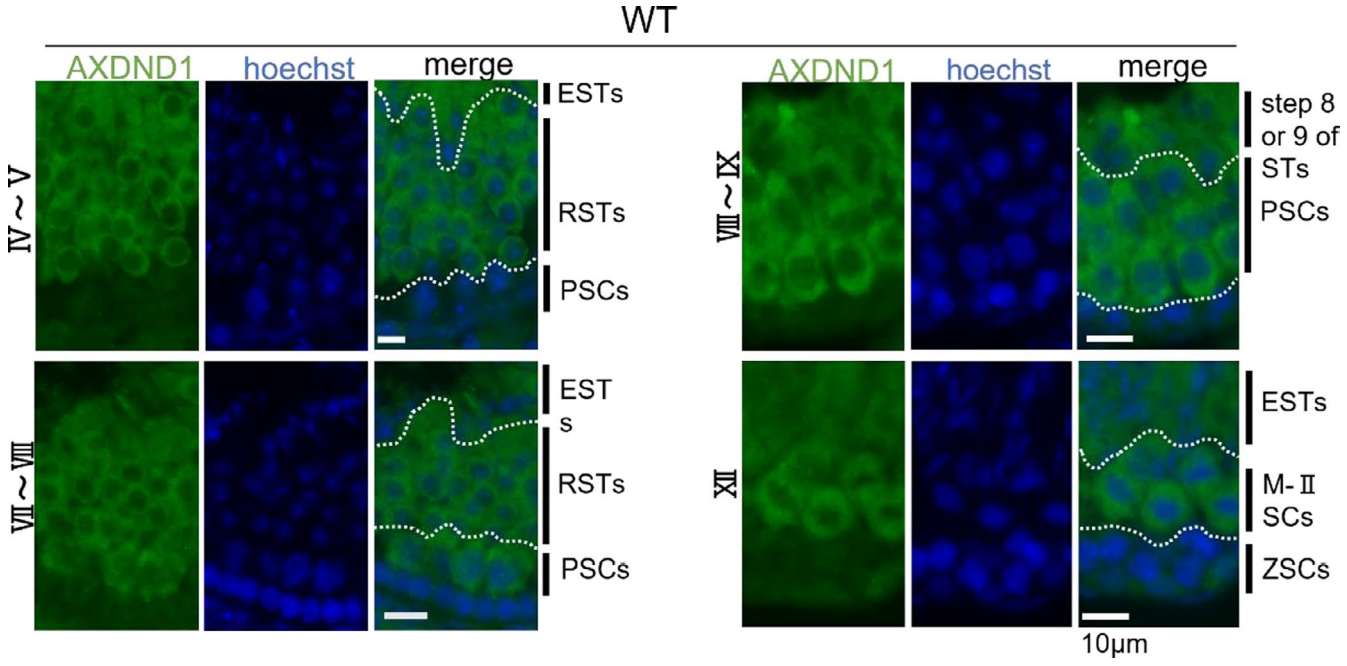

FIGURE 5 Staging of AXDND1 expression patterns in testicular sections. Staging of the seminiferous epithelium cycle with AXDND1 expression in WT testes (bars = 10 μm); AXDND1 (green), and DNA (blue). ESTs, elongated spermatids; M-IISCs, meiosis-II spermatocytes; PSCs, pachytene spermatocytes; RSTs, round spermatids; ZSCs, zygotene spermatocytes

the apoptotic frequency was counted using the TUNEL assay (Figure 2C). *Axdnd1*$^{-/-}$ testes showed significantly higher positive signals (*Axdnd1*$^{-/-}$ 119.7 ± 16.8 vs. WT 20.3 ± 4.73), indicating higher rates of apoptosis. Representative images of the TUNEL patterns are shown in Figure 2D.

Histological analysis revealed malformations during spermatid differentiation (Figure 3E,F). Elongated spermatids with malformed heads were detected in mutant mice at steps 10–12 of spermatid (panel of stage XII). After step 13, the number of spermatids decreased (panel of stage IV to V) and almost disappeared after step 15

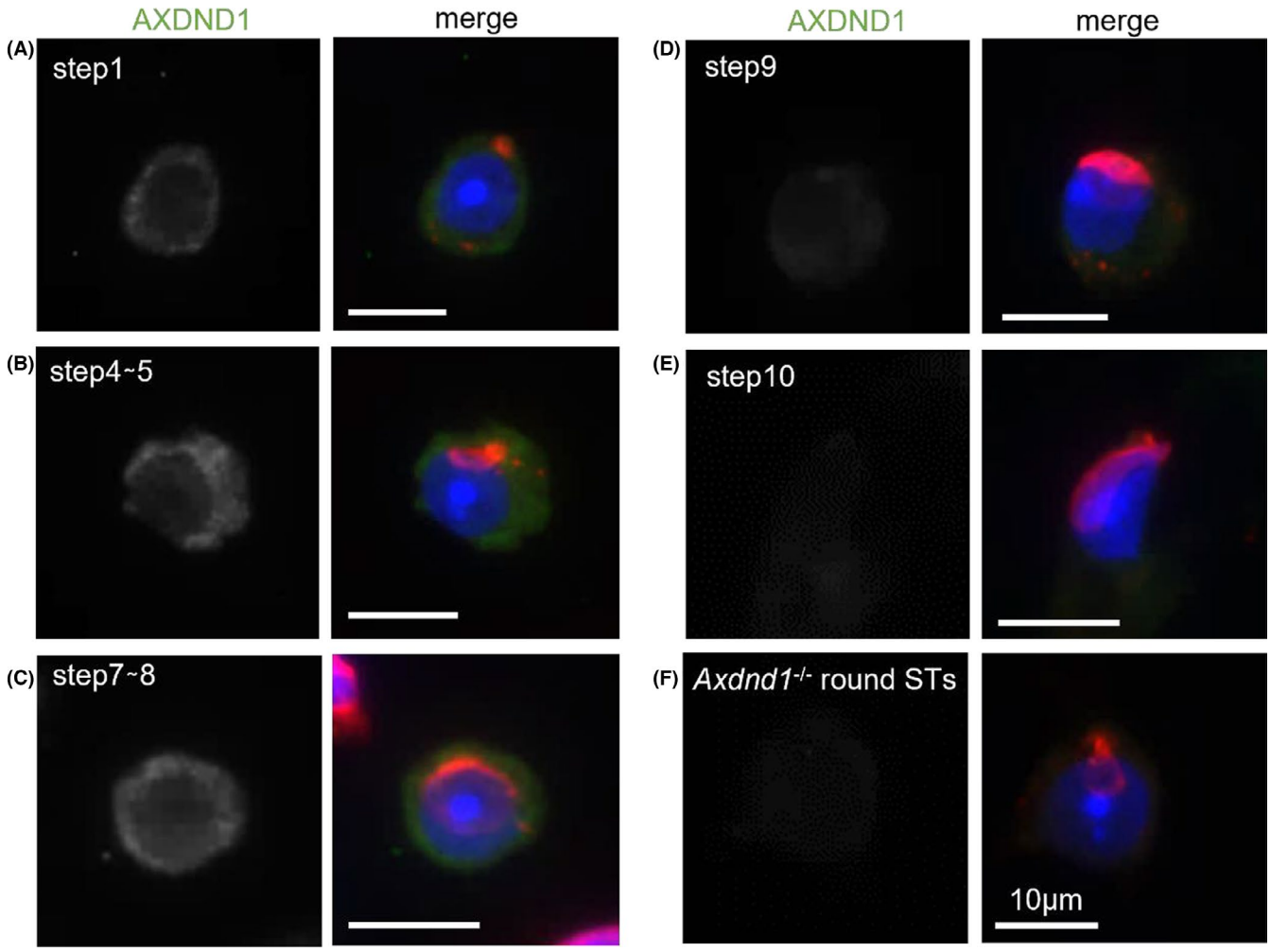

FIGURE 6 AXDND1 expression in early spermiogenesis. Expression patterns of AXDND1 during early spermiogenesis (steps 1 [A], 4 or 5 [B], 7 or 8 [C], 9 [D], and 10 [E]). AXDND1 (green), PNA (red), and DNA (blue). In the AXDND1 monochromatic panels on left side, signals are shown in gray for contrast. *Axdnd1*$^{-/-}$ round spermatids were used as a negative control. Bars = 10 μm

(panel of stage VII to VIII). Moreover, few spermatozoa were observed in the cauda epididymis (Figure 3G,H) and none retained their complete morphology (Figure 3I).

3.4 | Protein localization of AXDND1

Using a home-grown prepared rabbit polyclonal antibody, AXDND1 protein expression was analyzed in various tissues, revealing an intense signal in the testes and weak expression in the lungs and spleen (Figure 4A). Loss of AXDND1 expression in the mutant testes was observed (Figure 4B), and a specific immunostaining pattern was confirmed (Figure 4C).

Observations of different stages of seminiferous tubules demonstrated cytoplasmic expression of the protein from spermatocytes to elongated spermatids (Figure 5). AXDND1 signals were first detected in middle pachytene spermatocytes at stage VII. The signals remained throughout meiosis until early spermatids. Furthermore, immunocyte staining using testicular cells spread on glass also revealed that the AXDND1 expression was detected in spermatids until step 8 (Figure 6C), weakened in step 9 (Figure 6D), and almost disappeared in step 10 (Figure 6E).

3.5 | Abnormal manchette formation in the mutant testes

We investigated the malformation of spermatids and manchette structures of WT and *Axdnd1*$^{-/-}$ mice by immunostaining for α-tubulin (Figure 7). The manchette of elongating stage spermatids in *Axdnd1*$^{-/-}$ mice was abnormally longer (Figure 7E-G) or had disorganized tubulin structures (Figure 7H) compared to WT mice. These results indicated that AXDND1 participates in the formation of manchettes.

4 | DISCUSSION

The aim of this study was to understand the function of the uncharacterized protein AXDND1. *Axdnd1* mRNA expression was detected in the brain, lungs, spleen, and intestines, while low protein

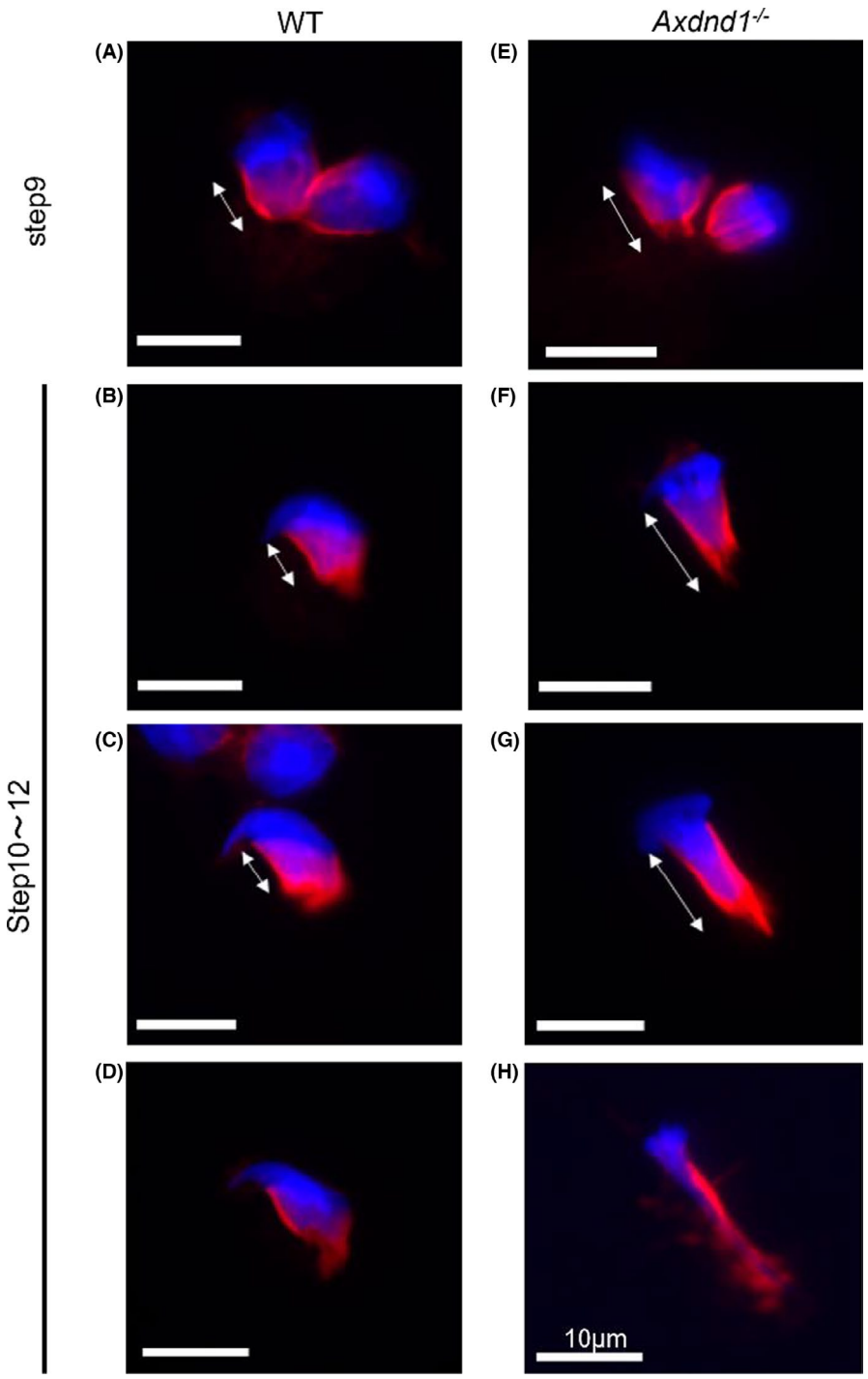

FIGURE 7 Abnormal formation of manchette structure in mutant testes. Immunostained manchette structures from elongating spermatids. Arrows indicate the length of the manchette between the peri- and post-nuclear directions. Representative WT or *Axdnd1*$^{-/-}$ spermatids of step 9 (A and E) and from steps 10 to 12 (B, C, D, F, G, and H). Some mutant spermatids had disorganized manchettes (H) compared to WT (D). α-tubulin (red) and nuclei (blue) are shown. Bars = 10 μm

expression was detected in both the lungs and spleen (Figure 1A). For many testicular flagellar genes, expression levels in the brain and lungs showed a similar pattern.

To uncover the contribution of *Axdnd1* to fertility, KO mouse models were generated, and we demonstrated that the loss of AXDND1 causes sterility (Table 1). The decrease in testes weight, explained by an increase in apoptosis, was confirmed by the TUNEL assay (Figure 2). In addition to spermiogenesis, AXDND1 may have functions involved in cell survival. Histological examination by PAS staining and immunohistochemistry further revealed malformation during sperm head formation and a lack of spermatids with a retained fine flagellar structure, indicating that sterility was induced by the degeneration of germ cells during spermatid differentiation (Figure 3).

Immunostaining with a usable home-grown antibody revealed cytosolic expression patterns from pachytene stage spermatocytes to round spermatids for the first time (Figure 5), which has not shown in the early study. According to a recent study[19] that used cells fractionated for each developmental stage, protein expression was detected in round spermatids but not in spermatocytes, which differs from the results of our microscopic examination. Since we could not find a description of how the

authors validated the purity of the enriched fraction, it is thought that this was due to differences in the protocol.

Axdnd1$^{-/-}$ spermatids showed a disorganized manchette structure (Figure 7); however, colocalization of AXDND1 was not observed in our immunocytochemical analysis. It is possible that the amount of protein distributed in the manchette was extremely small, below the limit of detection of the antibody, or that the effect on manchette formation could be determined in earlier steps. Given that *Axdnd1* plays a role in these early events, it is possible that microtubule aggregates appear and bind to related proteins.[11,22]

According to previous reports, dynein light chain proteins are involved in sperm motility. Dynein light chain 1 LC8 type 1 (DYNII1), a component of the dynein motor complex, was expressed during steps 9–16 of spermiogenesis in a rat model, in contrast to the AXDND1 expression pattern.[23] Another dynein light chain protein is the t-complex-coding protein DYNLT (*Tctex*). Both *Dynlt1* and *Dynlt2* were discovered in the t-haplotype allele, which is expressed in the sperm.[24–26] In human spermatozoa, a decrease in protein levels and loss of localization of DYNLT1 in flagella was observed in infertile patients; thus, DYNLT1 is thought to be a potential regulator of motility.[27] Targeting disruption of *Dyntl2*, one of the three copies of *Tcte3*, increased the frequency of apoptosis and decreased sperm motility.[28] One of the highlights of this study is that, unlike these light chain proteins, AXDND1 deficiency induces severe damage to the head and flagellar formation prior to its effects on motility. Phenotypic similarities have been reported in many gene KO mouse models. IFT proteins carry materials for flagellar building, and some gene mutants display disruption of head shaping.[4–6,29] Kinesin superfamily proteins also participate in axoneme building, and *Kif3a* inactivation in mouse spermatids results in abnormal manchette formation.[30] In addition, the ciliary protein Fused (STK36), a putative serine-threonine kinase, was shown to interact with KIF27.[31] Interactions of AXDND1 with these proteins should be evaluated in future studies.

In conclusion, we demonstrated that *Axdnd1* deficiency impairs the formation of the sperm head and flagella, suggesting it is a novel essential gene for spermiogenesis. The resulting phenotype differed from the predicted motility effects of the deficient phenotype of the known axoneme dynein light chain genes. This also includes the possibility that the role of the axonemal dynein light chain domain in AXDND1 is different or that other parts are responsible. Including the question why the disruption of Axdnd1 causes DNA damage, by demonstrating binding to relevant dynein heavy chains in the domain, the discovery of partner proteins and identification of their interacting binding sites will clearly explain and expand our understanding of spermiogenesis.

Moreover, according to recently reported results,[19] deleterious heterozygous mutations in *AXDND1* were found in non-obstructive azoospermia (NOA) patients. Therefore, *Axdnd1* is essential for human spermatogenesis. This indicates that *Axdnd1* deficiency may be the cause of NOA and that *Axdnd1* KO mice could be used as a model for future NOA studies. Here, we observed the behavior of AXDND1 using the antibody, which represents a major advance in elucidating the role of this protein. Further research using AXDND1-specific antibodies and a NOA mouse model is expected to make significant contributions to future NOA treatment options.

ACKNOWLEDGMENTS

Dr. M. Ikawa (Osaka University) provided helpful advice on the study plan.

CONFLICT OF INTEREST

The authors have no conflicts of interest directly relevant to the content of this study.

ANIMAL STUDIES AND APPROVAL BY ETHICS COMMITTEE

All animal experiments were approved by the Animal Care and Use Committee of the Research Institute of Tohoku University (2021 Agr-004). All the procedures involving animal experiments were performed according to the institutional and national guidelines for the care and use of laboratory animals.

ORCID

Kenshiro Hara https://orcid.org/0000-0001-8531-8349
Kentaro Tanemura https://orcid.org/0000-0003-4744-607X

REFERENCES

1. Lehti MS, Sironen A. Formation and function of the manchette and flagellum during spermatogenesis. *Reproduction*. 2016;151(4):43-54.
2. Rathke C, Baarends WM, Awe S, Renkawitz-Pohl R. Chromatin dynamics during spermiogenesis. *Biochem Biophys Acta*. 2014;1839(3):155-168.
3. Abou-Haila A, Tulsiani DR. Mammalian sperm acrosome: formation, contents, and function. *Arch Biochem Biophys*. 2000;389(2):173-182.
4. San Agustin JT, Pazour GJ, Witman GB. Intraflagellar transport is essential for mammalian spermiogenesis but is absent in mature sperm. *Mol Biol Cell*. 2015;26(24):4358-4372.
5. Zhang Y, Liu H, Li W, et al. Intraflagellar transporter protein (IFT27), an IFT25 binding partner, is essential for male fertility and spermiogenesis in mice. *Dev Biol*. 2017;432(1):125-139.
6. Liu H, Li W, Zhang Y, et al. IFT25, an intraflagellar transporter protein dispensable for ciliogenesis in somatic cells, is essential for sperm flagella formation. *Biol Reprod*. 2017;96(5):993-1006.
7. Ma DD, Wang DH, Yang WX. Kinesins in spermatogenesis. *Biol Reprod*. 2017;96(2):267-276.
8. Wu S, Li H, Wang L, et al. Motor proteins and spermatogenesis. *Adv Exp Med Biol*. 2021;1288:131-159.
9. Rosenbaum J, Witman G. Intraflagellar transport. *Nat Rev Mol Cell Biol*. 2002;3:813-825.
10. Ishikawa H, Marshall WF. Intraflagellar transport and ciliary dynamics. *Cold Spring Harb Perspect Biol*. 2017;9(3):a021998.
11. Sakai Y, Yamashita S. Mechanism for the removal of residual cytoplasm from spermatids during mouse spermiogenesis. *Anat Rec*. 1989;223(1):43-48.
12. Kierszenbaum AL, Tres LL. The acrosome-acroplaxome-manchette complex and the shaping of the spermatid head. *Arch Histol Cytol*. 2004;67(4):271-284.
13. Divina P, Vlcek C, Strnad P, Paces V, Forejt J. Global transcriptome analysis of the C57BL/6J mouse testis by SAGE: evidence for non-random gene order. *BMC Genom*. 2005;6:29.

14. Shima JE, McLean DJ, McCarrey JR, Griswold MD. The murine testicular transcriptome: characterizing gene expression in the testis during the progression of spermatogenesis. *Biol Reprod*. 2004;71(1):319-330.
15. Djureinovic D, Fagerberg L, Hallström B, et al. The human testis-specific proteome defined by transcriptomics and antibody-based profiling. *Mol Hum Reprod*. 2014;20(6):476-488.
16. Krausz C, Riera-Escamilla A. Genetics of male infertility. *Nat Rev Urol*. 2018;15(6):369-384.
17. Wang H, Yang H, Shivalila CS, et al. One-step generation of mice carrying mutations in multiple genes by CRISPR/Cas-mediated genome engineering. *Cell*. 2013;153(4):910-918.
18. Yan W. Male infertility caused by spermiogenic defects: lessons from gene knockouts. *Mol Cell Endocrinol*. 2009;306(1–2):24-32.
19. Ma Q, Cao C, Zhuang C, et al. AXDND1, a novel testis-enriched gene, is required for spermiogenesis and male fertility. *Cell Death Discov*. 2021;7(1):348.
20. Mokrina M, Nagasawa K, Kanamori M, Natsuike M, Osada M. Seasonal composition of immature germ cells in the Yesso scallop identified by *vasa*-like gene (*my-vlg*) and protein expression, with evidence of irregular germ cell differentiation accompanied with a high mortality event. *Aquac Rep*. 2021;19:100613.
21. Gurumurthy CB, Sato M, Nakamura A, et al. Creation of CRISPR-based germline-genome-engineered mice without ex vivo handling of zygotes by i-GONAD. *Nat Protoc*. 2019;14(8):2452-2482.
22. O'Donnell L, O'Bryan MK. Microtubules and spermatogenesis. *Semin Cell Dev Biol*. 2014;30:45-54.
23. Wang RA, Zhao M, Meistrich ML, Kumar R. Stage-specific expression of dynein light chain-1 and its interacting kinase, p21-activated kinase-1, in rodent testes: implications in spermiogenesis. *J Histochem Cytochem*. 2005;53(10):1235-1243.
24. Lader E, Ha HS, O'Neill M, Artzt K, Bennett D. tctex-1: a candidate gene family for a mouse t complex sterility locus. *Cell*. 1989;58(5):969-979.
25. Huw LY, Goldsborough AS, Willison K, Artzt K. Tctex2: a sperm tail surface protein mapping to the t-complex. *Dev Biol*. 1995;170(1):183-194.
26. Harrison A, Olds-Clarke P, King SM. Identification of the t complex-encoded cytoplasmic dynein light chain tctex1 in inner arm I1 supports the involvement of flagellar dyneins in meiotic drive. *J Cell Biol*. 1998;140(5):1137-1147.
27. Indu S, Sekhar SC, Sengottaiyan J, et al. Aberrant expression of dynein light chain 1 (DYNLT1) is associated with human male factor infertility. *Mol Cell Proteomics*. 2015;4(12):3185-3195.
28. Rashid S, Grzmil P, Drenckhahn JD, et al. Disruption of the murine dynein light chain gene Tcte3-3 results in asthenozoospermia. *Reproduction*. 2010;139(1):99-111.
29. Zhang Y, Liu H, Li W, et al. Intraflagellar transporter protein 140 (IFT140), a component of IFT-A complex, is essential for male fertility and spermiogenesis in mice. *Cytoskeleton*. 2018;75(2):70-84.
30. Lehti MS, Kotaja N, Sironen A. KIF3A is essential for sperm tail formation and manchette function. *Mol Cell Endocrinol*. 2013;377:44-55.
31. Nozawa YI, Yao E, Gacayan R, Xu SM, Chuang PT. Mammalian Fused is essential for sperm head shaping and periaxonemal structure formation during spermatogenesis. *Dev Biol*. 2014;388(2):170-180.

How to cite this article: Hiradate Y, Harima R, Yanai R, et al. Loss of *Axdnd1* causes sterility due to impaired spermatid differentiation in mice. *Reprod Med Biol*. 2022;21:e12452. doi:10.1002/rmb2.12452